Snow Particle Motion in Process of Cornice Formation

Hongxiang Yu $^{1,2},$ Li
 Guang 1, Benjamin Walter 4, Jianping Huang
 1, Ning Huang 2, and Michael Lehning
 3,4

Correspondence: Ning Huang (huangn@lzu.edu.cn)

Abstract. Snow cornices are a common snow pattern in cold regions, and their fracture and collapse can easily trigger avalanches. Despite numerous observations and experimental simulations on their formation process, the microscopic mechanism of their formation remains unclear. In this paper, based on wind-tunnel experiments and high-speed photography, experimental studies on the trajectory of particles surrounding the snow cornice were carried out. The experiment results reveal the distinct differences in particle size, impact velocity, and impact angle between the surface and the edge of a cornice. The findings show that the edge of a cornice is primarily composed of small snow particles. with saltation being the dominant movement pattern for particle adhesion. The distributions of impact velocity and angle of particles differ between the edge and the surface. The relative frequency of particle adhesion on the edge exponentially decreases with increasing impact velocity, while surface adhesion follows a Gaussian distribution. These differences are primarily attributed to topographic effects. Analysis of vertical impact velocity distributions reveals that both edge and surface particles follow the same exponential trend, with threshold velocities ranging from 2 to 2.5 m/s, indicating a similar adhesion mechanism. To further explain the observed differences in particle size between the edge and surface, the forces acting on particles adhering to the edge were analyzed. The results show that smaller or dendritic particles are more likely to adhere to the edge due to a higher cohesive-to-gravity force ratio (F_c/F_a) . Results indicated that the cornice is composed of small-sized snow particles. Saltation is the most dominant moving pattern for particles adhering to the cornice. Notably, pFurther analysis of force balance equations of particles at the edge explains the shape-forming mechanism of wedged-like snow cornice. This study quantitatively provides insights into the work enhances the understanding of the micro-mechanism of snow cornice formation, offering a theoretical foundation insights for improving avalanche prediction. The finding can be further generalized to address snow accumulations on mechanical structures, power lines, and other systems where similar force balance considerations are critical.

¹College of Atmospheric Science, Lanzhou University, Lanzhou, 730000, China

²College of Civil Engineering and Mechanics, Lanzhou University, Lanzhou, 730000, China

³College of Architecture Civil and Environmental Engineering, Ecole Polytechnique Federal de Lausanne, Lausanne, 1015, Switzerland

⁴WSL Institute for Snow and Avalanche Research SLF, Davos, 7260, Switzerland

NOTATION

Symbol	Definition and units
A	$Constant [=3.18 \times 10^{-7}]$
A_p	Projected area of one particle $[m^2]$
D	Diameter of particle [m]
$v_{ m p}$	Particle velocity [m s ⁻¹]
v_{px}	Particle velocity component in x direction $[m\ s^{-1}]$
v_{py}	Particle velocity component in y direction [m $\rm s^{\text{-}1}]$
v_{imv}	Vertical impact velocity of particle $[m\ s^{-1}]$
F_c	Cohesive force [N]
F_f	Frictional force [N]
F_g	Gravity force [N]
F_s	Supporting force [N]
M_s	Torque [Nm]
x	Radius of contact surface [m]
t	Current time [s]
Δt	Time step [s]
T_{air}	Air temperature $[^{o}C]$
$ heta_p$	Particle moving angle $[^o]$
$ heta_{im}$	Particle impact angle $[^o]$
θ	Cornice angle $[^o]$
α	Angle between direction of gravity and the x-axis
μ_f	Friction coefficient of ice surface
$ ho_p$	Particle density $[kg/m^3]$
σ	Tensile strength at failure [kPa]

1 Introduction

35

Snow consists of ice crystals. Snow particles may adhere to the surface at particle-bed collision. Therefore, wind can shape the snow cover and produce special patterns by redistributing snow over various areas, such as sastrugi, snow dunes (Sommer et al., 2018), and snow cornices (Seligman et al., 1936). Snow cornice is one of the naturally formed accumulation patterns in cold mountain regions. The collapse of snow cornices may induce snow avalanches (Vogel et al., 2012).

Previous field observations have consistently shown that the optimal wind speed range for cornice formation lies between one and two times the threshold wind speed (Eckerstorfer et al., 2013b; Vogel et al., 2012; Hancock et al., 2020). Recently, wind-tunnel experiments have further shown that cornice growth is maximized when the wind speed exceeds the threshold value by 40% (Yu et al., 2022). However, the micr-mechanism micro-mechanism for particle adhesion to the cornice edge has not been studied in detail, due to the difficulty in observing the formation process at the particle scale.

Currently, there are several hypotheses on how snow particles adhere at the edge: Irregularly-shaped snow particles interlock with each other by their dendrites (Seligman et al., 1936); Charged snow particles are attracted by the strong electric field above the snow cornice surface (Latham and Montagne, 1970); Pressure melt and frictional heat (Latham and Montagne, 1970) when particles contact other surfaces leads to a quasi-liquid layer facilitating fast sintering. In fact, when a particle impacts on a cornice surface, both the sintering time (10¹ s) and the fast-sintering time (10⁻¹ s)(Bahaloo et al., 20222) are much longer than the collision time (10⁻⁵ s). Thus, on the particle sintering/fast-sintering time scale, the drifting-snow aerodynamic process dominates the redistribution of snow particles and the patterns of snow cornices. However, the mechanicalmechanism behind the wedge-shaped (Seligman et al., 1936) snow cornice has not yet been investigated.

Cornice growth is often accompanied by drifting snow (Eckerstorfer et al., 2013a), in which a snow particle saltation layer exists. Drifting snow particles move in three modes, namely, creep, saltation, and suspension, with the first two modes contributing most to the snow mass transport (Bagnold, 2012). When snow particles collide with the surface, three processes may occur: 1) Rebound occurs when a portion of particle kinematic energy is lost, but may rebound from the surface; 2) Deposition occurs when the particle loses all its kinematic energy upon impact with the ground; 3) Eject occurs when the particle transfers the kinematic energy to other particles on the ground upon impact with surface, resulting in the entrainment of other particles resting on the surface.

During particle-surface collision, the particles transfer momentum and energy from the air to the surface. These processes are characterized using rebound and splash functions based on theoretical models (Lämmel et al., 2017; Comola and Lehning, 2017) or observations (Anderson and Haff, 1991). Particle impact velocity and impact angle (Walter et al., 2023) are two critical factors influencing key processes such asimportant parameters determining rebounding, deposition, and splashing. processes. These parameters play a significant role in determining how particles interact with surface upon collision. However, the specific method in which particle impact velocity and impact angle

influence particle adhesion, particularly in the context of snow cornice formation, remains poorly understood. Thus, investigation is needed to clarify the relationship between theses impact parameters and the mechanisms driving adhesion. It is however not clear how particle impact velocity and impact angle may affect particle adhesion snow cornice formation.

Here, we carry out a wind-tunnel experiment of cornice formation, focusing on particle trajectory and adhesion process in snow cornice formation. Based on the experimental results, we investigate the micro physical mechanism for cornice formation.

2 Instruments and methods

60

The wind-tunnel experiments are carried out in a ring wind tunnel in the cold lab of the WSL Institute for Snow and Avalanche Research, in Davos, Switzerland. The experiment setup is shown in Fig. 1. For tracing particle trajectories, a high-speed camera system is deployed. A feeding system is used to supply snow particles. The feeding rate of snow particles is manually kept stable. The snow particles are produced by a snow maker (Schleef et al., 2014). The geometrical diameters are 300 - 500 μm, and the shape of the snow crystals is dendritic, visually analyzed under a microscope. The room temperature of the cold lab is controlled and set at -5 °C, and the wind speed is kept at 4 m s⁻¹. The wind speed inside the wind tunnel is nearly uniform with a very thin (around 2 cm) boundary layer (Sommer et al., 2017; Yu et al., 2022). A ridge model with a fixed size (Fig. 1) is built with compacted snow before each experiment. A ridge model with a fixed size (height 0.125 m, total length 0.4 m, flat surface length 0.1 m) is built with compacted snow before each experiment, and its side view is shown in Fig. 1.

80 Before conducting the experiment, we have performed preliminary tests on both fresh snow particles and aged snow particles. Fresh snow particles, characterized by their highly dendritic shapes, were compared to decomposed snow particles, which are characterized by small rounded shapes after being stored for several days at a constant temperature of -10 °C. The results show that both types of snow particles are capable of forming a snow cornice. However, fresh snow particles exhibit a significantly higher propensity for cornice formation, as they are much easier to consolidate into a stable structure compared to aged snow particles. Therefore, fresh snow particles were used in the subsequent experiment.

The high-speed camera system consists of a high-speed camera (Phantom VEO710), an LED lamp as a light source, and a transparent plane positioned at the opposite side of the camera to diffuse the light source and achieve uniform illumination. The system is employed for shadowgraphy analysis. The shadowgraphy is a technique used for extracting the moving particle's size, velocity, and trajectory. It is similar to PTV (particle tracking velocimetry) (Baek and Lee, 1996; Tagliavini et al., 2022), which has the same algorithms for particle information, and it has been frequently used in recent snow-related studies, for its advantages in robustness, non-intrusiveness, and accessibility. Shadowgraphy is particularly suitable for tracking snow particles, which are partially transparent and irregular in shape. It has been successfully applied to measuring particle mass flux, velocity, and size distribution (Paterna et al., 2016; Walter

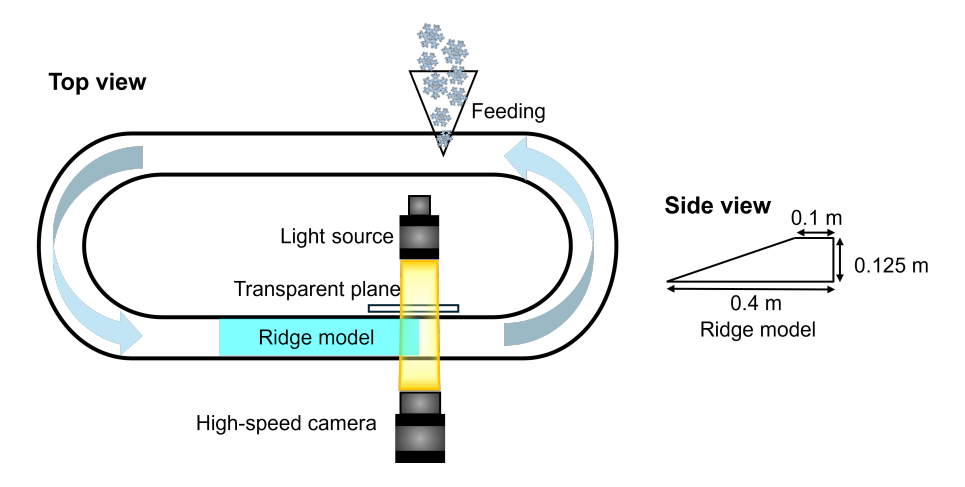


Figure 1. Schematic for experimental setups.

et al., 2023). The sampling frequency of the camera is set as 3 kHz, corresponding to a time interval of 333.32 µs. The images are captured for 4-5 s during cornice growth. In each case of the experiment, 12455 images are captured to record the particle trajectories. After the images are obtained, particle-bed collision events are selected visually. Then, particle sizes and trajectories in these events are analysed by image processing as follows.

2.1 Particle recognition

100

105

110

The gray value of the snow cornice base is much higher than that of airborne snow particles. Thus, the images are first transferred into binary format by the two threshold gray values to recognize both the snow cornice base and airborne snow particles. The cornice zone is detected according to the first threshold gray value. The airborne snow particles are then detected according to the second threshold gray value after extracting the cornice from the image.

Particle size as recognized by the first-time binary analysis using the second threshold gray value is normally smaller than its real size, as shown in Fig. 2(a)-(b). To compensate for the underestimated particle areas caused by binarization, a dilation process (Gonzalez and Woods, 2017) is applied after the binarization, which fills the small spaces around the snow particle and smooths the particle's boundary, as depicted in Fig. 2(c) and its zoomed-in counterpart in (d).

To distinguish the noise points from air-flow snow particles, opening and closing processes (Solomon and Breckon, 2011) are then operated. The opening process eliminates very fine objects (noise points) and smooths the snow cornice boundary, and the closing process corrects the image such as filling the tiny empty holes inside of the snow particles.

After the above image pre-processing, particle recognition is carried out by using the Seed-Filling Algorithm (SFA). SFA is an algorithm used to fill closed regions in an image. It starts from a seed point and gradually fills the regions adjacent to it with the same color until the boundary is reached. Snow particle area is calculated based on

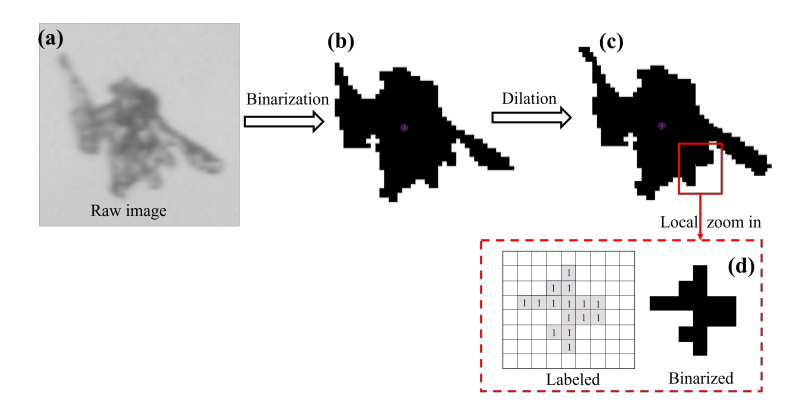


Figure 2. Image pre-processing method

the connected component label analysis (CCLA), a common image processing method for connecting the adjacent foreground pixels that have the same pixel value (Di Stefano and Bulgarelli, 1999; Rafael and Richard, 1993).

During the image processing, the particle's area is saved in binarized format in a numerical matrix. Thus, the particle's projected area A_p can be estimated by calculating the sum of all the connected component labels. The particle's equivalent diameter is calculated based on the value of its projected area: $d_e = \sqrt{4A_p/\pi}$. All pre-processing of images (dilation, opening, closing operations) and particle recognition in this work are programmed by using the Matlab software.

2.2 Particle trajectory tracking

125

130

By using the above particle recognition method, we obtained a series of images that contain the particle information.

Then, the trajectory and velocity of snow particles are obtained using the trajectory recognition method that judges the relative position of the neighboring particles.

We paired each particle from the previous time series of images, by using the nearest-neighbor algorithms (NNA) (Crocker and Grier, 1996) to match the targeted particle's position in each frame image. NNA is a particle search method as shown in Fig. 3. In each time step, we search for the position of the target particle in the last frame of an image within the predefined search radius. The center of the corresponding circle area is assumed to be at the mass center of the target particle in the last frame, and the radius is 6 mm. We then match the target particle by its shadow surface area similarity. By recognizing the position of the target particle in each frame image, we obtain the velocity of the target particles.

The $k_{th}i_{th}$ target particle's horizontal and vertical velocity at a given time step t and a time interval Δt is calculated as:

$$v_{px}(t) = \frac{x(t + \Delta t) - x(t)}{\Delta t} \tag{1}$$

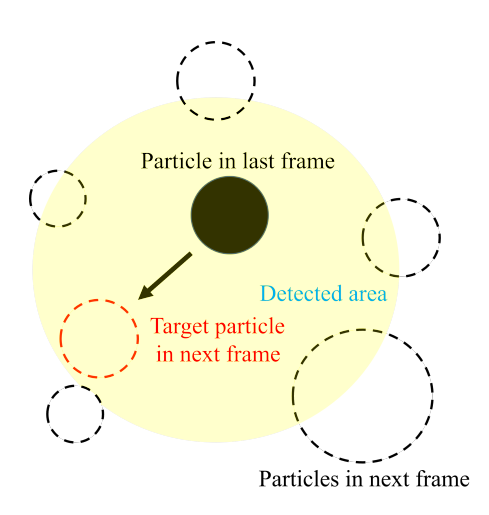


Figure 3. Schematic of particle detection method in post-processing high-speed camera images. The full circle is the particle from the last frame, the dashed circle is the particles from the second frame, and the yellow region is the predefined search area.

$$v_{py}(t) = \frac{y(t + \Delta t) - y(t)}{\Delta t} \tag{2}$$

in which x and y are the coordinate positions in x-axis and y-axis, t is the current time, and Δt is the time interval of a high-speed camera. Therefore, the magnitude of particle velocity $w_i v_p$ is:

$$v_p(t) = \sqrt{v_{px}(t)^2 + v_{py}(t)^2} \tag{3}$$

where v_{px} and v_{py} are the velocity component in x and y direction, respectively. The particle moving angle θ_p can be calculated as:

$$\theta_p(t) = \arctan(\frac{v_{py}(t)}{v_{nx}(t)}) \tag{4}$$

A particle contact event is defined when the particle's vertical velocity is from negative (downward) to zero or positive (upward) among several adjacent images. The impact velocity is then defined as the velocity before the contact, and the rebound velocity is defined as the velocity after the contact. We found the maximum error between visual observation (manually tracking the particle's trajectory) and program recognition of the edge particle velocity to be about 5%, the angle to be about 18%, and the diameter to be about 16%.

145 3 Results and discussions

150

155

160

By maintaining the wind speed in the experiment at constant (4 m/s), 190 collision particles are analyzed with the image post-processing method, in which, 65 particles adhere to the cornice edge and 86 particles adhere to the cornice upper surface. By maintaining the wind speed in the experiment at a constant (4 m/s), the study analyzed 655 collision particles interacting with the snow surface. These interactions included particles that rebounded, impacted, or deposited on the snow, as determined through an image post-processing method. Among these particles, 186 adhered to the cornice edge, while 469 adhered to the cornice upper surface. The cornice edge herein this paper refers to the spatial range of the 1 mm vertical front end of a dynamically growing cornice, and the cornice surface refers to the cornice's topside with the total length at the current time step minus the edge length, as is shown in Fig. 4(a).

The distributions of the snow particle impact velocity, impact angle, and size distribution are shown in Fig. 4(b). The blue points represent the particles that adhere to the edge and the red points represent those that adhere to the surface. The size of all points represents the particle's diameter. It can be concluded that the impact angle decreases with the increasing impact velocity. P particles that adhere to the edge have relatively lower and more narrowly-distributed values of impact velocity, but widely-distributed impact angle, compared to the particles that adhere to the surface. To investigate the differences between edge and surface particles, we analyzed the adhere particle's size distribution, impact velocity, and impact angle in the following sections.

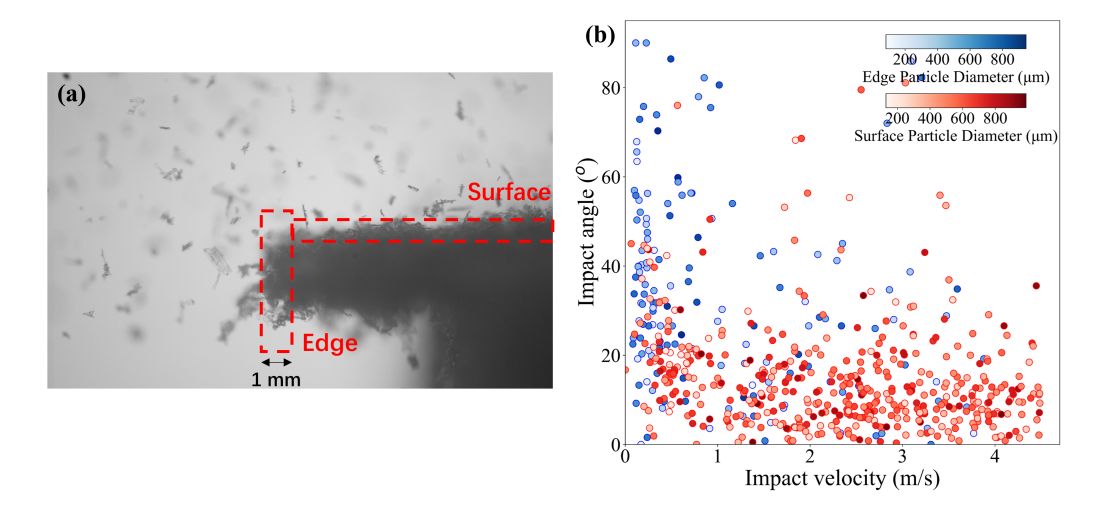


Figure 4. (a) Cornice edge and surface, with the dashed box indicating the regions of edge and surface. (b) Impact velocity and impact angle of snow particles of different sizes (deeper color represents larger size) on edge (in blue points) and surface (in red points).

3.1 Particle size distribution

165

The size distribution of particles adhering at different positions on a dynamically evolving cornice is analyzed, as is shown in Fig. 5. For all particles adhering to the cornice surface, their size distribution follows the Log-normal distribution described by $\theta \sim N(\mu=277.17, \theta=0.45)$, with the average diameter $\overline{D_{all}}=340$ um. For particles adhering at the edge, their size distribution follows the Log-normal distribution described by $\theta \sim N(\mu=264.42, \theta=0.38)$, with the average diameter $\overline{D_{edge}}=329$ um. And fFor particles adhering on the surface, their size distribution follows the Log-normal distribution function described by $\theta \sim N(\mu=342.69, \theta=0.28)$, with the average diameter $\overline{D_{surface}}=405$ um. It can be concluded that particles with smaller sizes adhere more likely on the edge, and larger particles adhere more likely on the cornice surface.

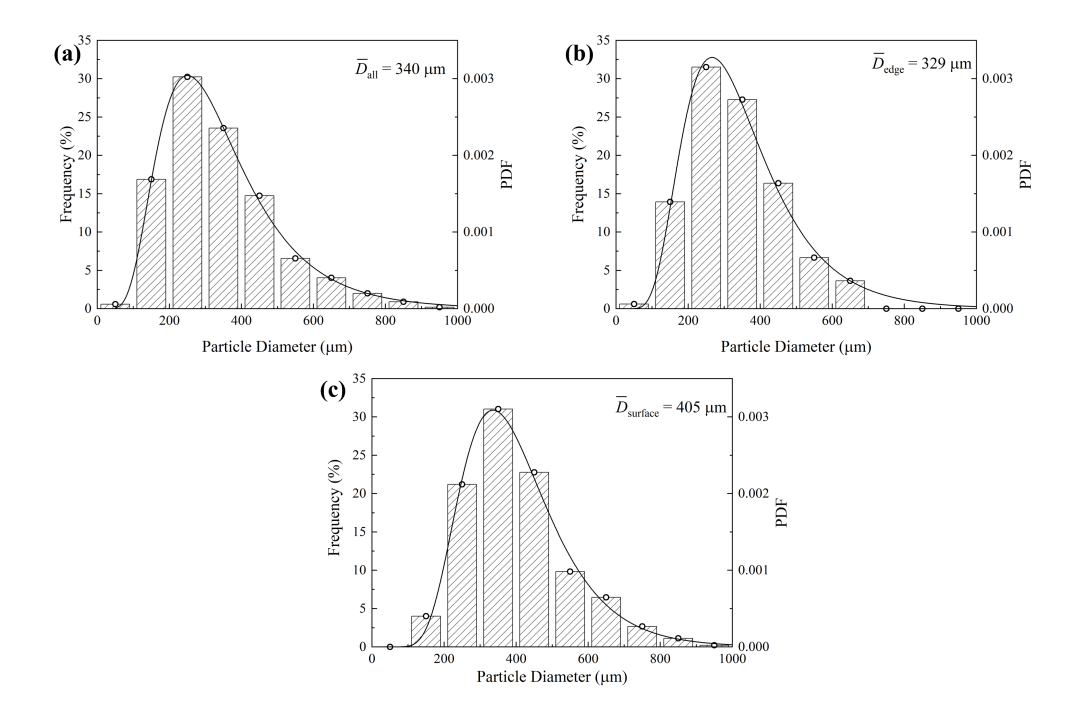


Figure 5. Size distribution of particles at different positions. (a) Airborne particles. (b) Adhesion particles at the edge. (c) Adhesion particles on the surface. The gray shadow represents the existence frequency of particles with different sizes.

The observed differences in particle size distribution across various locations suggest that environmental conditions, such as fluid field and gravitational effect, play an important role in influencing the adhesion of particles of different sizes. The flow on the cornice surface is a boundary layer flow, which provides a more stable environment with less turbulence, facilitating the deposition of larger particles. In contrast, the flow on the edge is a separation flow, where the ability to counteract particle gravity differs. On edge, larger particles are more likely to fall due to gravity, while

175 smaller particles can stay on edge under cohesive adhesion force. Moreover, smaller particles, with better followability with the wind, are more likely to stay on edge under the influence of the reflux vortex behind the cliff.

The Stokes number (normally defined as $St = \frac{\rho_p d^2 U}{18\mu L}$) is a ratio of inertial effects to diffusive effects of a particle. For particles adhering on the edge, the Stokes number is ≈ 1.8 , thus those edge particles are dominant by the inertial force. The Stokes number of the surface particle is ≈ 3.1 , which is about 1.7 times greater than that of the edge particle, indicating that the inertial effect is more significant on the surface particle than on the edge particles.

3.2 Particle movement pattern

180

185

190

195

In the experiment, the suspended particles in the higher region of the observation window fly over the cornice with a relatively high horizontal velocity and have little chance to deposit on the cornice, and almost all adhering particles reach the cornice edgetip first by saltating or creeping at the surface and then stop at the edge. Thus, Here, we mainly captured the particles moving very close to the surface by using a high-speed camera. It is observed that creeping (particle rolling or sliding over the surface before stop) and saltating (particle successively jumping over the surface before settling) (Bagnold, 2012) are the two main types of particles contributing to the growth of the cornice. Creeping particles are entrained from the surface under the ejection of other particles. These creeping particles (~13.6%about 14%) normally have larger sizes and lower velocities. After undergoing multiple rotations in the downstream direction, some of the creeping particles come to a stop near the front end of the cornice, as is shown in 6(a), and some of them keep rolling until they reach the edge and roll over.and some of them continue rolling to the edgetip and roll over the edgetip. Only a few creeping particles with elongated dendrites were found to physically interlock with adjacent particles at the front end of the cornice. Under the action of gravity, the hanging particles may start rotation with the interlocking point as the force center, as shown in Fig. 6(b), process 2-4.

Whether saltating particles rebound or deposit on the cornice surface after impaction is depends strongly influenced by on their impact position, velocity, and angle. Among all the particles that settle on the cornice surface, $\sim 82.3\%$ about 82% are saltating particles that deposit before reaching the cornice's front end, Most of the saltating particles deposit ($\sim 82.3\%$ about 82%) before the cornice's front end, as is shown in Fig. 6(c). Only a few of particles deposit on the front end, which are smaller-sized particles ejected near the edgetip. Fewer saltating particles ($\sim 3.4\%$ about 3%) going off the edgetip will later move backward to the cornice edgetip, under the action of the reflux vortex or the potential electric field, as shown in Fig. 6(d).

3.3 Particle impact velocity and angle

Here, we define the impact velocity/angle of the particle that deposits on the cornice surface as particle adherence velocity/angle (PAV/PAA). We first analyze the PAV and PAA of 469 particles deposited on the surface and 186 particles deposited on the edge.the 65 particles deposited on the edge and 86 particles deposited on the surface. In

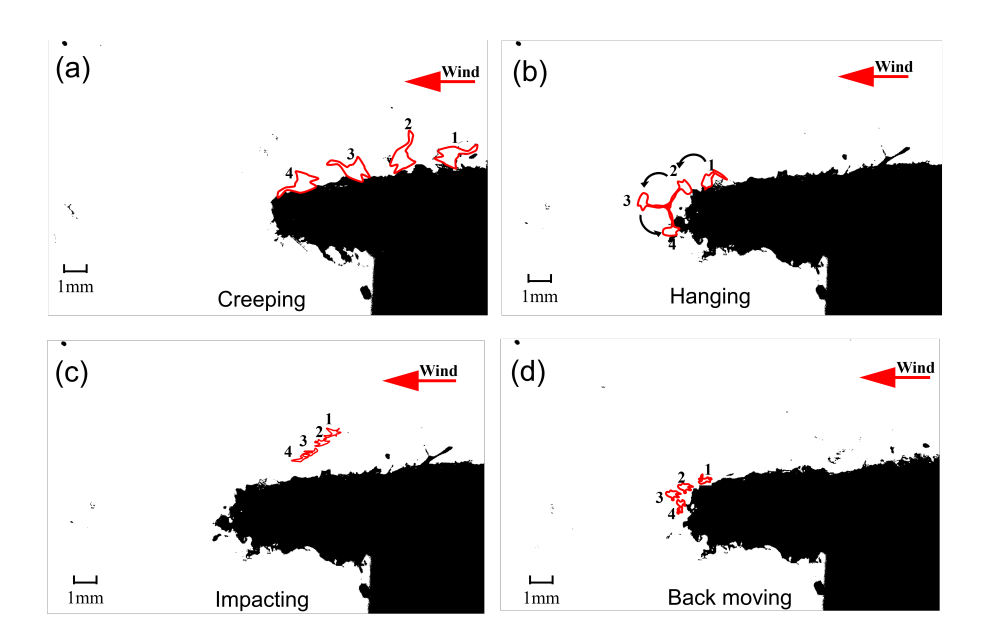


Figure 6. Four adhering patterns of snow particles (1,2,3,4 represents for different time steps).(a) Creeping particles. (b) Hanging particles. (c) Impacting particles. (d) Back moving particles.

natural conditions, the snow cornice will slowly bend and deform under the gravity force. In our experiment, the snow cornice can be considered as horizontally growing in the whole process, and the bending effect of the snow cornice can be neglected for the short observation time. The impact angle is defined as the angle of particle incidence on the horizontal cornice surface. We subdivided the values of particle impact velocity and impact angle into different bins and analyzed the relative frequency of these values. The average value of each bin is plotted as dots and the standard deviation is plotted as error bars in Fig. 7.

210

215

220

The relative frequency of PAV/PAA represents the probability of particle adhesion on the cornice with a certain impact velocity or impact angle. It is shown in Fig. 7(a) that for edge particles, the two types of particles, the adhesion probability exponentially decreases with the increasing value of PAV. The upper limit value is 4 m/s for the surface particles and 1.5 m/s for edge particles. Specifically, the relative frequency of the edge PAV follows the exponential function $f(v_{im}) = 4.3 + 30e^{-0.9v_{im}}$ ($R^2 = 0.96$). This indicates that particles with lower impact velocities are more likely to adhere to the edge. The majority of edge particle adhesion occurs at velocities below 1.5 m/s, highlighting the critical role of low-velocity impacts in cornice growth. $f(v_{im}) = -0.03 + 0.64e^{-2.49v_{im}}$ ($R^2 = 0.89$) and While the relative frequency of the surface PAV follows the the Gaussian distribution exponential function of $f(v_{im}) = -2.8 + \frac{79}{3.4\sqrt{\pi/2}}e^{-2(\frac{v_{imp}-2.9}{3.4})^2}(R^2 = 0.91)$, with values mainly concentrated at 3 m/s. This indicates that particles deposited on the surface normally have a higher impact velocity than the edge. The low number of particles adhering to the surface at low impact velocities can be attributed to the wind speed in the wind tunnel, which is set at 4 m/s. At this

225 wind speed, the majority of particles are entrained and transported at higher velocities, leaving only a small fraction of particles moving at very low velocities near the cornices surface. $f(v_{im}) = -0.08 + 0.72e^{-1.32v_{im}}(R^2 = 0.98)$

Thus, the rebound probability of particles on surface is $f_{re}(v_{im}) = 1 - f_{st}(v_{im}) = 1.08 + 0.72e^{-1.32v_{im}}$, and the rebound probability of particles on edge is $f_{re}(v_{im}) = 1 - f_{st}(v_{im}) = 1.03 + 0.64e^{-2.49v_{im}}$. The rebound probability functions are both exponential functions of the impact velocity, which is consistent with the previous research (Anderson and Haff, 1991).

As is shown in Fig. 7(b) that the frequency of PAA of surface particles follows the Exponential distribution function $f(\theta_{im}) = -0.8 + 80.6e^{-0.1v_{imp}}$ ($R^2 = 0.97$), with values mainly concentrated below 17°. While the frequency of PAA impact angle of edge particles follows the Gaussian distribution function $f(\theta_{im}) = 7.1 + \frac{448.8}{45.7\sqrt{\pi/2}}e^{-2((v_{imp}-18.1)/45.7)^2}$ ($R^2 = 0.72$), with values distributed more uniformly in range. The average value of PAA the impact angle of surface particles is 13°, which is consistent with the previous experimental results of Nishimura and Hunt (2000), as is shown in the red dash in Fig. 7(b).

Furthermore, we combined the impact velocity and angle by analyzing the vertical impact velocity $(v_{imv} = v_{im} sin \theta_{im})$ in Fig. 7(c). Both surface particles and edge particles follow the exponential distribution, with surface particles $f_s(v_{imv}) = 0.5e^{-v_{imv}/0.7}(R^2 = 0.96)$, and edge particles $f_s(v_{imv}) = -0.1 + 0.5e^{-0.9v_{imv}}(R^2 = 0.95)$. Particles adhere at low vertical impact velocities, whether on edges or surfaces. For both edge and surface particles, the threshold vertical impact velocity ranges from 2-2.5 m/s, with edge particles having a lower threshold velocity compared to surface particles.

It is noted that the vertical impact velocity distributions of surface particles and edge particles are in the same trend, although the impact velocity and impact angle distributions of edge particles and surface particles are different. It indicates that particle adhesion is mainly determined by the vertical impact velocity, and the differences in impact velocity and angle distributions between surface and edge is due to the fluid field differences caused by topographic changes.

3.4 Static force analysis of adhering particles on the cornice edge

230

240

245

250

255

The cornice growth process can be divided into two stages (Yu et al., 2022). The first stage is the formation of a 1-2 particle-diameter thick snow slab, which is mainly determined by the spatial variation in the mass transport rate along the flow direction. The second stage is a repeated process of length growth and then thickness growth.

From the above work, we statistically characterized the kinematic properties of the moving particles around the snow cornice. However, the mechanics of particles stopping and adhering at the cornice edge have not been examined in detail. We now discuss the process of particle deposition at the edge by analyzing the balance of the static forces acting on the particles.

Considering the differences in particle size distribution between the edge particles and surface particles, we conducted a static analysis of the particles at the edge. As shown in Fig. 8, consider a newly deposited particle i adhering to the foremost particle j at the edge of the cornice. Particle i is subjected to gravity F_q , the cohesive force F_c exerted

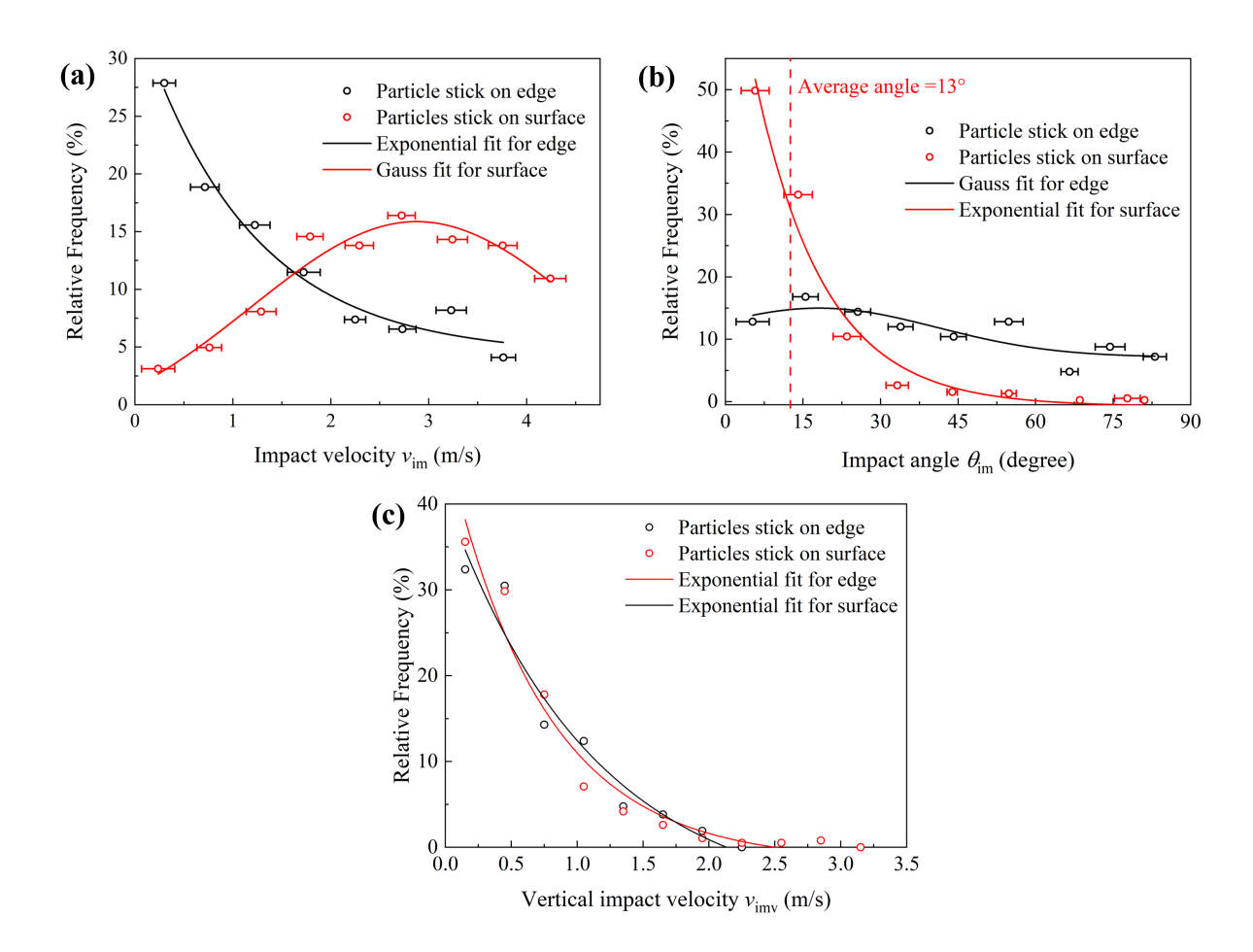


Figure 7. Relative frequencies of (a) particle adherence velocity PAV, (b) particle adherence angle PAA, and (c) the vertical impact velocity of particles on edge and surface.

by particle j, and the frictional force F_f at the contact surface. Due to the separation of flow, the wind velocity and surface shear stress near the edge of the cornice are close to zero (DeBonis, 2022; Shehadi, 2018), allowing the drag and lift forces acting on particle i to be neglected compared to other forces (Schmidt, 1980).

Considering one particle (particle j) at the edge of the cornice and one newly deposited particle (particle i), as depicted in Fig. 8. The drag force and the lift force acting on particle i can be neglected due to the near-surface velocity and surface shear stress at the edges being close to zero.

The overlap area represents the compression deformation surface of the two particles.

260

265

The force balance equations for particle i can expressed as: By considering the center point on the surface as the analyzed balance point, the force and torque balance of particle i can be expressed as:

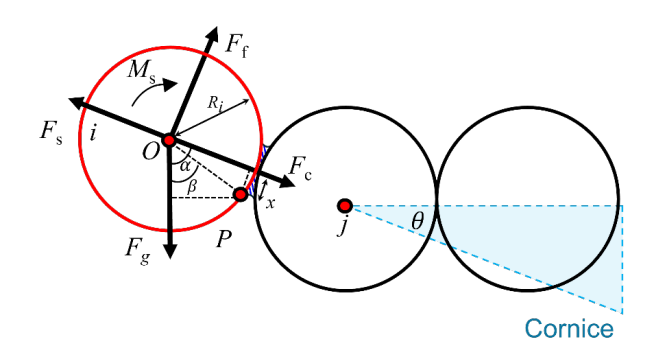


Figure 8. Schematic diagram of force analysis of particles adhering onto the edge.

$$F_q \cos \alpha + F_c = F_s \tag{5}$$

$$270 \quad F_q \sin \alpha \le F_f \tag{6}$$

$$F_f = \mu_f F_s \tag{7}$$

Here, F_g is the gravity force on particle i, F_c is the cohesive bond force, which is $\pi x^2 \sigma$ (Szabo and Schneebeli, 2007), where σ is the tensile strength at failure and x is the radius of the bond (blue shadowed area). F_s is the supporting force. α is the angle between the direction of gravity and cohesive force. R_i is the radius of particle i.

When snow particles adhere to the surface, both the gravity force F_g and the adhesive force F_c are in the vertical direction, resulting in an upward support force from the surface that maintains their stationary position. However, when snow particles adhere to the edge, the gravity force F_g and the adhesive force F_c are not in the same direction. The component of the cohesive force in the direction of the gravity force is balanced by the support force generated by the edge, while the component of the gravity force perpendicular to the adhesive force needs to be balanced by friction force F_f . Once this component exceeds the frictional force, the particles will fall.

By substituting Eq. (5) and Eq. (7) into Eq. (6), we can derive the condition for particle i to maintain mechanical equilibrium if:

$$\frac{F_c}{F_g} \ge \frac{\sin \alpha}{\mu_f} - \cos \alpha \tag{8}$$

To analyze the stability of particle i, overturning moments are calculated around point P (at the edge of the bond). The supporting force F_s and cohesive force F_c act through the center of particle i and operate on point P through

285

the moment arm x. The gravity force F_g acts on point P through the moment arm $Rsin(\alpha - arcsin(x/R))$, where the angle between F_g and line \overline{OP} (distance from particle center to point P) is $\beta = \alpha - arcsin(x/R)$. The friction force F_f acts on point P through the moment arm Rcos(arcsin(x/R)). The condition for the particle to remain in equilibrium is $M_s \leq 0$. Therefore:

290

305

$$(F_s - F_c)x + F_g R sin(\alpha - arcsin(\frac{x}{R})) - F_f R cos(arcsin(\frac{x}{R})) \le 0$$

$$(9)$$

Substituting Eq. (5) and Eq. (7) into Eq. (9) yields:

$$\frac{F_c}{F_g} \ge \frac{x/R \cdot cos\alpha + sin(\alpha - arcsin(x/R)) - \mu_f cos\alpha cos(arcsin(x/R))}{\mu_f cos(arcsin(x/R))} \tag{10}$$

Given the bond radius $x \ll R(Gubler, 1982)$, it follows that $x/R \sim 0$ and $\arcsin(x/R) \sim 0$. Thus, we can simplify the Eq. (10) to:

$$\frac{F_c}{F_g} \ge \frac{\sin\alpha}{\mu_f} - \cos\alpha \tag{11}$$

Eq. (11), derived from the momentum equilibrium analysis, is consistent with Eq. (8), which is derived from the force balance analysis. This equation indicates that particles adhering to the edge within the range of $[0, \alpha]$ can remain stable. The ratio of cohesive force (F_c) to gravity force (F_g) is proportional to the upper limit of angle α , indicating that a higher cohesive force or lower gravity force results in a wider stable angle range for α .

Dendritic snow particles, which have a cohesive force approximately 1.44 times greater than that of spherical particles (Eidevag et al., 2022), exhibit a larger angle α . This larger angle indicates a broader range of balanced positions at the edge, making dendritic particles more prone to adhering at the edges. This tendency explains the experimental phenomenon that fresh snow is more likely to form snow cornices.

Additionally, smaller snow particles experience lower gravity forces. Consequently, the ratio of Fc to Fg is higher, leading to increased values of α and enhancing their tendency to adhere. This finding aligns with the results of this experiment, that smaller snow particles are more likely to adhere at the edges.

inwhich, F_g is the gravity force on particle i, F_c is the cohesive force between two particles, α is the angle between the direction of gravity and cohesion, D is the diameter of particle i. δ_{max} is the maximum compression displacement of the particle that can be calculated with the model proposed by Zhou (2011): δ_{max} = (1.25πR_i^{2.5}R_j^{2.5}ρ_p² (1-μ_i²)E_i (π_i+π_j(R_i²-R_iR_j+R_j²) with R_{i/j} is the radius of two contact particles, ρ_p is particle density, E_{i/j} and μ_{i/j} are the Yong's modulus and the Poisson's ratio of particles, μ_f is the friction coefficient of the ice surface, and Δl is the horizontal growth length
which is lower than the diameter of particle i.

The angle of the cornice θ is the complementary angle of α , and it is therefore affected by particle size D and air temperature T. As the air temperature T increases or the particle size D decreases, the ratio of $\frac{F_c}{F_g}$ rises, and

the cohesive force F_c dominates over the gravity force F_g . Under this condition, the cornice is stable even with a relatively small angle θ . On the other hand, the gravity force F_g dominates over the cohesive force F_c when the air temperature is low or particle size is large, and the shape of the cornice can only be stable with a large angle θ . This result is consistent with the previous experiment (Yu et al., 2022)

4 Conclusions

320

325

330

335

340

345

In this work, the micro-mechanism of snow cornice formation is investigated in a wind-tunnel experiment. Using a high-speed camera system, we recorded and analyzed particle trajectories surrounding the cornice, facilitated by a novel snow particle recognition program.

Our findings reveal that near-surface saltation and creeping are the primary modes for particles to adhere to the cornice. Among the adhered particles, the majority are saltating particles that settle on the surface, while only a few deposit directly at the front end. Additionally, some creeping particles interlock and hang with others at the cornice edge, and a small number of particles may detach from the edge and move backward due to opposing forces acting against the flow. These varying movement patterns of particles contribute to the increase in both the thickness and length of the cornice, which is essential for its structural growth.

The experiment results show that although the distributions of the size, impact velocity, and impact angle of particles on surface and edge are different, the vertical impact velocity distribution is consistent, with threshold velocities ranging from 2 to 2.5 m/s for adhesion. Quantitative analysis demonstrates that the relative frequency of edge particle adhesion decreases exponentially with impact velocity, while surface adhesion follows a Gaussian distribution. This indicates that the particle adhesion is dominated by the vertical impact velocity. The variations in particle size, impact velocity, and impact angle distributions arise from the distinct fluid field generated by sudden topographic change.

Moreover, the cornice edge is primarily composed of lightweight snow particles compared to the cornice surface. This phenomenon can be attributed to the mechanics of particle adhesion, where the ratio of cohesive forces to gravity forces plays a critical role. Smaller particles, particularly dendritic ones, are more likely to adhere to the edge due to their favorable physical properties (with higher F_c/F_g ratios), which enhance their stability in the presence of wind and other forces.

Overall, this research provides valuable insights into the micro-mechanisms of snow cornice formation, emphasizing the critical roles of particle size, movement patterns, and environmental conditions. The findings have important implications for avalanche prediction and management, as understanding snow cornice dynamics can help mitigate risks associated with their fracture and collapse in cold regions. Furthermore, these insights may extend to related phenomena, such as the formation of snow bridges of ice crevasse, wire icing, and snow accumulation on train bogies, highlighting the broader relevance of particle adhesion mechanisms. Future studies should continue to explore

350 the interactions between environmental factors and particle behavior to refine our understanding of snow cornice dynamics.

We then analyzed the static force balance for particles adhering to the edge of the cornice. The force balance suggests that the cornice angle is determined by the ratio of cohesive force and gravity force, which is influenced by air temperature and particle size.

In this work, the topography of the simulated mountain ridge featured an ascending slope leading to a flat expanse at its summit. This increasing slope induced flow separation at the edge, resulting in diminished wind velocity. Such conditions potentially elevate the probability of particle deposition. Future works should quantitatively study the influence of ridge morphology on cornice formation through experimental wind tunnel or numerical simulation.

Author contributions. YHX designed the experiments. YHX and LG carried out the experiments. YHX performed the data analysis, and prepared the first draft. ML, BW, HJP and HN reviewed and edited the paper. HN and ML organized this study, contributed to its conceptualization, discussion, and finalized the paper.

Competing interests. The authors declare that they have no conflict of interest.

Data availability. The data archiving is underway and will be added after it is published. Data is available on request now.

Acknowledgements. The authors would like to thank the WSL Institute Snow and Avalanche Research SLF for making the experimental facilities available for our study. We thank Alec van Herwijnen for his invaluable experiment support. This work was supported by the National Natural Science Foundation of China (grant no.: U22A20564), the Third Comprehensive Scientific Expedition and Research Program in Xinjiang (grant no.: 2022xjkk0101), the Second Tibetan Plateau Scientific Expedition and Research Program (grant no.: 2019QZKK020109-2), and the Swiss National Science Foundation (grant 200020-179130). The data and code will be uploaded to the Dryad repository after the paper is published. Additionally, we are deeply grateful to the two anonymous reviewers and two scholars (Li Hongyi and Li Bailiang) for their insightful comments and constructive suggestions, which have greatly contributed to improving the quality and clarity of this paper.

References

390

400

405

- Anderson, R. S. and Haff, P. K.: Wind modification and bed response during saltation of sand in air, in: Aeolian grain transport 1, pp. 21–51, Springer, 1991.
- Baek, S. J. and Lee, S. J.: A new two-frame particle tracking algorithm using match probability, Experiments in Fluids, 22, https://doi.org/10.1007/BF01893303, 1996.
 - Bagnold, R. A.: The physics of blown sand and desert dunes, Courier Corporation, 2012.
 - Comola, F. and Lehning, M.: Energy- and momentum-conserving model of splash entrainment in sand and snow saltation, Geophysical Research Letters, 44, 1601–1609, https://doi.org/10.1002/2016GL071822, 2017.
- 380 Crocker, J. C. and Grier, D. G.: Methods of Digital Video Microscopy for Colloidal Studies, Journal of Colloid and Interface Science, 179, 298–310, https://doi.org/https://doi.org/10.1006/jcis.1996.0217, 1996.
 - DeBonis, J.: A Large-Eddy Simulation Of Turbulent Flow Over A Backward Facing Step, https://doi.org/10.2514/6.2022-0337, 2022.
- Di Stefano, L. and Bulgarelli, A.: A simple and efficient connected components labeling algorithm, in: Proceedings 10th

 385 International Conference on Image Analysis and Processing, pp. 322–327, https://doi.org/10.1109/ICIAP.1999.797615,
 1999.
 - Eckerstorfer, M., Christiansen, H. H., Vogel, S., and Rubensdotter, L.: Snow cornice dynamics as a control on plateau edge erosion in central Svalbard, Earth Surface Processes and Landforms, 38, 466–476, 2013a.
 - Eckerstorfer, M., Christiansen, H. H., Vogel, S., and Rubensdotter, L.: Snow cornice dynamics as a control on plateau edge erosion in central Svalbard, Earth Surface Processes and Landforms, 38, 466–476, 2013b.
 - Gonzalez, R. C. and Woods, R. E.: Digital Image Processing 4th Edition, Pearson; 4th edition, 2017.
 - Hancock, H., Eckerstorfer, M., Prokop, A., and Hendrikx, J.: Quantifying seasonal cornice dynamics using a terrestrial laser scanner in Svalbard, Norway, Natural Hazards and Earth System Sciences, 20, 603–623, https://doi.org/10.5194/nhess-20-603-2020, 2020.
- 395 Latham, J. and Montagne, J.: The possible importance of electrical forces in the development of snow cornices, Journal of Glaciology, 9, 375–384, publisher: Cambridge University Press, 1970.
 - Lämmel, M., Dzikowski, K., Kroy, K., Oger, L., and Valance, A.: Grain-scale modeling and splash parametrization for aeolian sand transport, Physical Review E, 95, 022 902, https://doi.org/10.1103/PhysRevE.95.022902, 2017.
 - Nishimura, K. and Hunt, J. C. R.: Saltation and incipient suspension above a flat particle bed below a turbulent boundary layer, Journal of Fluid Mechanics, 417, 77–102, https://doi.org/10.1017/S0022112000001014, 2000.
 - Paterna, E., Crivelli, P., and Lehning, M.: Decoupling of mass flux and turbulent wind fluctuations in drifting snow, Geophysical Research Letters, 43, 4441–4447, 2016.
 - Rafael, G. and Richard, W.: Digital Image Processing, in: Digital Image Processing, pp. 57–68, 1993.
 - Schleef, S., Jaggi, M., Löwe, H., and Schneebeli, M.: An improved machine to produce nature-identical snow in the laboratory, Journal of Glaciology, 60, 94–102, https://doi.org/10.3189/2014JoG13J118, 2014.
 - Schmidt, R. A.: Threshold Wind-Speeds and Elastic Impact in Snow Transport, Journal of Glaciology, 26, 453–467, https://doi.org/10.3189/S0022143000010972, 1980.

- Seligman, G., Seligman, G. A., and Douglas, C.: Snow structure and ski fields: being an account of snow and ice forms met with in nature, and a study on avalanches and snowcraft, Macmillan and Company, limited, 1936.
- 410 Shehadi, E.: Large Eddy Simulation of Turbulent Flow over a Backward-Facing Step, Ph.D. thesis, https://doi.org/10.13140/RG.2.2.17703.24480, 2018.
 - Solomon, C. J. and Breckon, T.: Fundamentals of Digital Image Processing: A Practical Approach with Examples in Matlab, 2011.
- Sommer, C. G., Lehning, M., and Fierz, C.: Wind tunnel experiments: saltation is necessary for wind-packing, Journal of Glaciology, 63, 950–958, https://doi.org/10.1017/jog.2017.53, 2017.
 - Sommer, C. G., Wever, N., Fierz, C., and Lehning, M.: Investigation of a wind-packing event in Queen Maud Land, Antarctica, The Cryosphere, 12, 2923–2939, https://doi.org//10.5194/tc-12-2923-2018, 2018.
 - Szabo, D. and Schneebeli, M.: Subsecond sintering of ice, Applied Physics Letters, 90, 151 916–151 916, https://doi.org/10.1063/1.2721391, 2007.
- Tagliavini, G., Khan, M. H., Mccorquodale, M., Westbrook, C., and Holzner, M.: Wake characteristics of complex-shaped snow particles: Comparison of numerical simulations with fixed snowflakes to time-resolved particle tracking velocimetry experiments with free-falling analogs, Physics of Fluids, 34, 055 112, https://doi.org/10.1063/5.0089759, 2022.
 - Vogel, S., Eckerstorfer, M., and Christiansen, H. H.: Cornice dynamics and meteorological control at Gruvefjellet, Central Svalbard, The Cryosphere, 6, 157–171, https://doi.org/10.5194/tc-6-157-2012, 2012.
- Walter, B., Weigel, H., Wahl, S., and Löwe, H.: Wind tunnel experiments to quantify the effect of aeolian snow transport on the surface snow microstructure, The Cryosphere Discussions, 2023, 1–27, https://doi.org/10.5194/tc-2023-112, 2023.
 - Yu, H., Li, G., Walter, B., Lehning, M., Zhang, J., and Huang, N.: Environmental Conditions for Snow Cornice Formation tested in a Wind Tunnel, The Cryosphere, pp. 1–15, https://doi.org/10.5194/tc-2022-27, 2022.